Available online at www.sciencedirect.com
ScienceDirect
Journal of Computational Physics 225 (2007) 2069–2082
JOURNAL OF COMPUTATIONAL PHYSICS
www.elsevier.com/locate/jcp

An adaptive homotopy multi-grid method for molecule orientations of high dimensional liquid crystals

Ping Lin [a], Thomas Richter [b,*]

[a] Department of Mathematics, The National University of Singapore, Singapore 117543, Singapore
[b] Department for Aeronautics and Astronautics, Massachusetts Institute of Technology, Cambridge, MA 02139, USA

Received 14 September 2006; accepted 9 March 2007
Available online 24 March 2007

Abstract

The liquid crystal molecule orientation is arranged by minimizing the so-called Oseen–Frank energy functional. For a better understanding of these complicated orientation singularities, simplified models resulting from specific choices of elastic constants are always of interest. In this paper a pseudo Newton method together with a multi-grid linear system solver or preconditioner is used to compute the orientation of liquid crystal molecules based on a simplified Oseen–Frank energy functional. The penalty method is used to deal with the unit-length constraint of liquid crystal molecules. The Newton and multi-grid methods do not converge when some parameters are small. A homotopy algorithm combined with mesh refinement strategies in order to deal with small parameter cases is studied and is found to be very robust in computing the solution of the model. The method is implemented to compute the orientation of liquid crystal molecules in domains of typical shapes and with various rotational boundary conditions in 2D and 3D. Interesting singularity patterns are observed.

MSC: 65H20; 65N55; 65N30; 76A20

Keywords: Multigrid; Homotopy; Liquid crystals; Adaptivity

1. Introduction

Liquid crystals are a phase of matter whose order is intermediate between that of a liquid and that of a crystal. The molecules are typically rod-shaped with a fixed length and their ordering is important to characterize their microstructure. The nematic phase, for example, is characterized by the orientational order of the constituent molecules. Nematics are the most commonly used phase in liquid crystal displays (LCDs), with many such devices using the twisted nematic geometry.

* Corresponding author. Tel.: +1 617 997 7107.
E-mail addresses: matlinp@math.nus.edu.sg (P. Lin), trichter@mit.edu (T. Richter).

0021-9991/$ - see front matter © 2007 Elsevier Inc. All rights reserved.
doi:10.1016/j.jcp.2007.03.009

There is growing interest in the theory of liquid crystals among physicists and mathematicians due to their broad applications. There exists a number of phases in liquid crystals. The study of phases and transition phenomenon between them (e.g. from nematic to smectic-A) is thus an important topic in the theory of liquid crystals (see [10,11]). Classical Oseen–Frank theory (cf. [13]) suggests that the nematic phase of liquid crystals can be described by a director field $\mathbf{n}$, which minimizes the following Oseen–Frank energy functional

$$\mathscr{W}(\mathbf{n}) = \int_\Omega W(\mathbf{n}, \nabla\mathbf{n})\,\mathrm{d}\mathbf{x},$$

where $\Omega \subset \mathbf{R}^i$, $i = 2$ or 3, is a bounded domain occupied by the liquid crystal sample, and

$$W(\mathbf{n}, \nabla\mathbf{n}) = \frac{k_1}{2}|\nabla\cdot\mathbf{n}|^2 + \frac{k_2}{2}|\mathbf{n}\cdot\nabla\times\mathbf{n}|^2 + \frac{k_3}{2}|\mathbf{n}\times\nabla\times\mathbf{n}|^2 + \frac{k_2+k_4}{2}[tr(\nabla\mathbf{n})^2 - (\nabla\cdot\mathbf{n})^2].$$

Here the k_i are elastic constants and $k_1, k_2, k_3 > 0$ are splay, twist and bend constants, respectively. The molecular orientation can be controlled with applied forces on the boundary. So we shall consider Dirichlet boundary conditions. The last term $[tr(\nabla\mathbf{n})^2 - (\nabla\cdot\mathbf{n})^2]$ will be dropped, since it is a divergence term and can be reduced to a surface integral via integration by parts (see [17], Lemma 1.2). So we only need to consider

$$W(\mathbf{n}, \nabla\mathbf{n}) = \frac{k_1}{2}|\nabla\cdot\mathbf{n}|^2 + \frac{k_2}{2}|\mathbf{n}\cdot\nabla\times\mathbf{n}|^2 + \frac{k_3}{2}|\mathbf{n}\times\nabla\times\mathbf{n}|^2. \tag{1}$$

As pointed out in [11] the full form of (1) is still too complex to be of practical use – either because the relative values of the three elastic constants k_i are unknown, or because the equilibrium equations derived from (1) are prohibitively difficult to solve. Indeed, no theoretical analysis has been done to the general Oseen–Frank functional. In such cases, a further simplification based on specific choices of elastic constants is often useful to understand the orientation pattern. There are two typical simplifications. If $k_1 = k_2 = k_3 = 1$ then the Oseen–Frank energy becomes

$$\mathscr{W}(\mathbf{n}) = \frac{1}{2}\int_\Omega |\nabla\mathbf{n}|^2\,\mathrm{d}\mathbf{x}. \tag{2}$$

Together with a fixed length condition, say $|\mathbf{n}| = 1$, the solution is also called harmonic map from a 2D or 3D compact manifold to a 2D circle or 3D sphere, respectively. Some basic numerical results and techniques have been reported in [1,8,9,15]. It is also related to phase field models in dealing with moving interface and image processing problems if changing $\mathbf{n}$ to a scalar phase field variable. There are also other studies on the coupling of the simplified model (2) with flow field in 2D (see, e.g. [12,20,21]). If $k_2 = k_3 = k + k_1$, we can have another simplification

$$\mathscr{W}(\mathbf{n}) = \frac{1}{2}\int_\Omega [k_1|\nabla\mathbf{n}|^2 + k|\nabla\times\mathbf{n}|^2]\,\mathrm{d}\mathbf{x}. \tag{3}$$

Although the assumption on the ratio of parameters k_i may not be quantitatively true in various practical situations, this simpler form of (1) resulting from the assumption is often a valuable tool to reach a qualitative insight into material properties such as molecule orientations. It is expected that, as $k \to \infty$, the asymptotic behavior of minimizers of (3) under suitable boundary conditions will provide a mathematical representation of the phase transition process of liquid crystals from nematic phase to smectic-A phase (see [16,19]). Some mathematical analysis for the limiting case of (3) is discussed in [2,3,17,18,22]. That is why we are particularly interested in considering the limiting case that $k \gg k_1$. It is also very challenging to design appropriate numerical methods in this case since the ellipticity of the operator is largely reduced. Some initial numerical results in simple 2D cases are reported in [14] where the direct method is used to solve the resulting linear system.

In this paper we will focus on the simplified model (3) since not many theoretical and numerical results are available. We will mainly consider three dimensional cases with $k \gg k_1$. In 3D and, in particular, when more nodes are needed due to the orientation singularities there is no hope to use a direct method to solve the linear system resulted from the Newton's iteration of this nonlinear problem. We shall use the multigrid method to solve the linear system or use it as a pre-conditioner for an iterative linear system solver

(such as conjugate gradient or GMRES) since the problem is a vector elliptic equation. However, the iterative method is often not convergent due to the small parameter k_1/k and the small penalty parameter for the unit length constraint. We thus propose a homotopy method on these small parameters to increase the accuracy of the initial guess of the iterative method. It turns out that the homotopy method together with the Newton-multigrid iteration works very robustly for this liquid crystal model. We shall first consider the model in a square or a rectangular in 2D and then a cubic or parallelepiped domain in 3D, as well as on a spherical or an ellipsoidal domain where the boundary is smooth. By choosing various winding boundary data we observe various interesting orientation solutions, their singularity patterns and evolution from a given initial guess to the steady state solution. We hope that our observations will help with the understanding of the orientation of liquid crystal molecules and motivate further theoretical study of the solution of this liquid crystal model. All numerical examples are solved with the PDE library *Gascoigne* [7].

2. Formulation of the problems

Let Ω be a bounded domain of $\mathbb{R}^2$ or $\mathbb{R}^3$. We denote by Γ the boundary of Ω, and we suppose that Γ is sufficiently smooth (for example, Lipschitz-continuous). Define the space $\mathbf{H}^1(\Omega) = (H^1(\Omega))^i$ and $\mathbf{L}^2(\Omega) = (L^2(\Omega))^i$, $i = 2$ or 3, and denote $\epsilon = k_1/k$. We can write the energy functional (3) as

$$J_\epsilon(\mathbf{n}) = \frac{1}{2}\int_\Omega [\epsilon|\nabla \mathbf{n}|^2 + |\nabla \times \mathbf{n}|^2]\,d\mathbf{x}, \quad \forall \mathbf{n} \in \mathbf{H}^1(\Omega), \tag{4}$$

where ϵ should be a small positive constant. Note that $\mathbf{n}$ in (3) satisfies a Dirichlet boundary condition and is a director vector, namely, its length is one. So we look for solutions in the set:

$$S = \{\mathbf{n} | \mathbf{n} \in \mathbf{H}^1(\Omega), \quad \mathbf{n} = \mathbf{g} \text{ on } \Gamma, \quad |\mathbf{n}| = 1\text{a.e.}\}, \tag{5}$$

where $|\mathbf{n}| = (n_1^2 + n_2^2 + n_3^2)^{\frac{1}{2}}$. The boundary data $\mathbf{g}$ is a unit vector field such that $S \neq \varnothing$.

With the above notation, we consider the following minimization problem

$$\text{Find } \mathbf{u} \in S, \quad \text{such that} \quad J_\epsilon(\mathbf{u}) \leqslant J_\epsilon(\mathbf{v}), \quad \forall \mathbf{v} \in S. \tag{6}$$

The unit vector constraint $|\mathbf{v}| = 1$ makes it a non-convex minimization problem. We can have three ways to deal with the constraint, namely projection, Lagrangian multiplier and penalty methods. We are not going to use the method of Lagrange multipliers since it would lead us to a kind of generalized eigenvalue/eigenfunction problem which may be more complicated to solve than projection and penalty methods. The projection method is numerically simple but its theoretical formulation involves a so-called "subgradient" which is not a mathematically well-understood subject (see [14]). The penalty method is a favorable way for PDE analysts since the resulting system is more regular to researchers and the limiting argument may possibly be applied to study the properties of the solution. So we shall use the penalty formulation in our computation as well.

The penalty formulation of (6) reads:

$$\begin{cases} \text{Find} \quad \mathbf{u} \in \mathbf{H}_g^1, \quad \text{such that} \\ J_\epsilon(\mathbf{u}) + \frac{1}{4\eta}\int_\Omega (|\mathbf{u}|^2 - 1)^2\,d\mathbf{x} \leqslant J_\epsilon(\mathbf{v}) + \frac{1}{4\eta}\int_\Omega (|\mathbf{v}|^2 - 1)^2\,d\mathbf{x}, \quad \forall \mathbf{v} \in \mathbf{H}_g^1. \end{cases} \tag{7}$$

The variational formulation for the liquid crystal model is

$$\begin{cases} \text{Find} \quad \mathbf{u} \in \mathbf{H}_g^1, \quad \text{such that,} \\ \epsilon\int_\Omega \nabla \mathbf{u} : \nabla \mathbf{v}\,d\mathbf{x} + \int_\Omega (\nabla \times \mathbf{u}) \cdot (\nabla \times \mathbf{v})\,d\mathbf{x} + \frac{1}{\eta}\int_\Omega (|\mathbf{u}|^2 - 1)\mathbf{u} \cdot \mathbf{v}\,d\mathbf{x} = 0, \quad \forall \mathbf{v} \in \mathbf{H}_0^1(\Omega), \end{cases} \tag{8}$$

where $\eta > 0$ is another small parameter associated with the penalty method for the unit-length constraint. We also note that the term associated with the *curl* operator can be replaced by the term associated with the *grad* and *div* operators, since

$$\int_\Omega (\nabla \times \mathbf{u}) \cdot (\nabla \times \mathbf{v})\,d\mathbf{x} = \int_\Omega \nabla \mathbf{u} : \nabla \mathbf{v}\,d\mathbf{x} - \int_\Omega (\nabla \cdot \mathbf{u})(\nabla \cdot \mathbf{v})\,d\mathbf{x}, \forall \mathbf{v} \in \mathbf{H}_0^1(\Omega). \tag{9}$$

We shall use a finite element method to approximate problem (8). Suppose that $\Omega \subset \mathbb{R}^2$ or $\mathbb{R}^3$. Using a quadrilateral (or hexahedral) finite element triangulation of $\overline{\Omega}$ being denoted as $\mathscr{T}_h = \{T\}$, we approximate $\mathbf{H}^1$ and $\mathbf{H}^1_0$ by the finite element spaces

$$\mathbf{V}_h = \{\mathbf{v}_h \in \mathbf{C}^0(\overline{\Omega}), \mathbf{v}_h|_T \in Q_1(T), \forall T \in \mathscr{T}_h\},$$

and

$$\mathbf{V}_{gh} = \{\mathbf{v}_h \in \mathbf{V}_h, \mathbf{v}_h = \mathbf{g}_h \text{ on } \Gamma\},$$

respectively. Here $Q_1(T)$ is the space of the polynomials resulting from an iso-parametric mapping of a reference element $\widehat{T} = [0,1]^2$ or $\widehat{T} = [0,1]^3$ respectively, to the element T of degree $\leqslant 1$. Also $\mathbf{V}_{0h}$ is the particular case of $\mathbf{V}_{gh}$ with $\mathbf{g}_h = \mathbf{0}$. For the case of non-polygonal boundaries we use higher order mappings of the reference element onto the computational elements T in order to reduce the approximation error along the boundaries (see [6] for a complete description of the finite element spaces).

3. The multigrid method and homotopy

For abbreviation we write the discrete variational system of (8) (replacing the functional spaces $\mathbf{H}^1_0$ by $\mathbf{V}_{0h}$ and $\mathbf{H}^1$ by $\mathbf{V}_{gh}$, respectively) as: finding $\mathbf{u}_h \in \mathbf{V}_{gh}$ such that

$$a(\mathbf{u}_h)(\mathbf{v}_h) = 0, \quad \forall \mathbf{v}_h \in \mathbf{V}_{0h}, \tag{10}$$

using the nonlinear form $a(\cdot)(\cdot)$. To solve this problem, we shall use a pseudo Newton method. Starting with an initial guess $\mathbf{u}^0_h$ (usually the interpolation of the solution on a coarser triangulation) we get iterates $\mathbf{u}^n_h$ by successively following Algorithm 1.

Algorithm 1. Newton iteration

Require: initial guess $\mathbf{u}^0_h$, error tolerance τ, matrix parameter α

1: **for** $n = 0$ **to** N **do**
2: calculate residual $d^n_h = a(\mathbf{u}^n_h)(\cdot)$
3: calculate norm $\rho^n = \|d^n_h\|$
4: **if** $\rho^n \leqslant \tau$ **then**
5: **break**
6: **end if**
7: **if** $\rho^n/\rho^{n-1} \geqslant \alpha$ **then**
8: build system matrix $A_h = a'_u(\mathbf{u}^n_h)(\cdot,\cdot)$
9: **end if**
10: solve linear system $A_h(\mathbf{u}^{n+1}_h - \mathbf{u}^n_h) = -d^n_h$
11: **end for**

Until a given tolerance τ for the residual is reached in step 4, the Jacobian in step 8 of the Newton iteration is only newly assembled, if the convergence rate of the preceding step was bad (usually we take $\alpha \approx 0.2$). With $a'_u(\cdot)(\cdot,\cdot)$ we indicate the Frechet derivative of the nonlinear form $a(\cdot)(\cdot)$:

$$a'_u(\mathbf{u})(\mathbf{w},\phi) := \frac{\mathrm{d}}{\mathrm{d}t} a(\mathbf{u} + t\mathbf{w})(\phi)\bigg|_{t=0}. \tag{11}$$

The resulting linear system in step 10 of the Newton iteration will be solved using a multi-grid method due to its fast convergence for elliptic problems. For the multi-grid iteration we are using the V-cycle with about 8 smoothing steps each for pre- and post-smoothing.

As smoother we apply a block-wise incomplete LU decomposition without any fill-in. We locally block all degrees of freedom belonging to one mesh node. In particular the local nonlinearities due to the penalty term demand for this coupling. For a further stabilization of the ILU decomposition we add fractions of off diagonal entries to the diagonal one. For coarse meshes up to about 5000 degrees of freedom a fast direct solver is applied.

To enhance the robustness of the linear solver, this multi-grid iteration is used as a pre-conditioner for a conjugate gradient solver.

Even for a moderate choice of the two parameters ϵ and η in Eq. (8) the nonlinear as well as the linear problems are a challenge to the numerical methods. For small values of the parameter ϵ, the influence of the Laplacian, hence the elliptic character is reduced and the kernel of *curl* gets significant. As consequence, the convergence rate of the linear solver is worsened.

The nonlinear penalty term induces "singularities" to the solution. In combination with a small value of ϵ, very sharp fronts appear within the solution, where the orientation of the crystals turns, and the length collapses to zero. These fronts are that sharp, that the solution is not educible on coarse meshes.

Algorithm 2. Homotopy Newton iteration

Require: initial guess $\mathbf{u}_h^0$, error tolerance τ, matrix parameter α, initial homotopy parameter η^0, homotopy limit η_{lim}, homotopy control γ_1, γ_2, β.

1: **for** $n = 0$ **to** N **do**
2: calculate residual $d_h^n = a(\mathbf{u}_h^n)(\cdot)$
3: calculate norm $\rho^n = \|d_h^n\|$
4: **if** $\rho^n \leqslant \tau$ **then**
5: **break**
6: **end if**
7: **if** $\rho^n/\rho^{n-1} \leqslant \gamma_1$ **and** $\rho^n/\rho^{\text{last}} \leqslant \gamma_2$ **then**
8: reduce $\eta = \beta\eta$
9: calculate residual $d_h^n = a(\mathbf{u}_h^n)(\cdot)$
10: calculate norm $\rho^n = \|d_h^n\|$
11: set $\rho^{\text{last}} = \rho^n$.
12: **end if**
13: **if** $\rho^n/\rho^{n-1} \geqslant \alpha$ **then**
14: build system matrix $A_h = a'_u(\mathbf{u}_h^n)(\cdot,\cdot)$
15: **end if**
16: solve linear system $A_h(\mathbf{u}_h^{n+1} - \mathbf{u}_h^n) = -d_h^n$
17: **end for**

The immediate solution of the problem with small parameters is often not possible. Remedy might be the usage of a time stepping scheme of a gradient flow or a hydrodynamic liquid crystal model with zero velocity field (cf. [14,20]). However, this results in very long solving times, especially considering three dimensional problems.

Here, we propose the combination of the Newton solver with a homotopy method: while solving the nonlinear problems we successively adjust the parameters ϵ and η. For the control of the (homotopy-)parameters η and ϵ as well as the size of the meshes a detailed analysis of the Newton convergence behavior will be used.

For simplification we present out method considering one homotopy parameter η. We start with some large value $\eta = \eta_{\text{start}}$ and want to reach η_{lim}. If the Newton convergence is good, that is, if the reduction rate ρ^n/ρ^{n-1} is small, we reduce the homotopy parameter. To prevent that the method tends to an unstable solution we further demand a certain overall reduction of the residual since the last reduction step. The homotopy Newton iteration is described in Algorithm 2.

The parameter γ_1 in step 7 indicates the tolerance for "good convergence". We usually choose $\gamma_1 \approx 0.1$. The second condition is necessary to assure that the Newton method converges to the correct solution. By reducing the parameters to rapidly the solution might run into unstable local minima. We set $\gamma_2 \approx 10^{-4}$.

The reduction factor β in step 8 is usually chosen as $\beta \approx 0.5$–0.75.

If the parameter η gets small (compared to the size of the mesh elements), the condition $\rho^n/\rho^{\text{last}} \leqslant \gamma_2$ in step 7 will never be fulfilled. Then we will keep the current homotopy parameter until the Newton tolerance in step 4 is reached. On the next refinement level, a further reduction of the parameter is possible.

In the next section we will give examples for the convergence progress of this homotopy method.

3.1. Numerical analysis of the homotopy method

We analyze the homotopy method in detail for the following configuration. Considering the 3D spherical domain we use the boundary (and initial) conditions

$$u^x(r,\theta,\phi) = \sin(\theta)\sin(2\phi),$$
$$u^y(r,\theta,\phi) = \sin(\theta)\cos(2\phi),$$
$$u^z(r,\theta,\phi) = \cos(\theta).$$

Starting with a prolongation of the boundary values into the domain, the classical Newton iteration ceases work even for the relatively large choice of parameters $\eta = 0.1$ and $\epsilon = 0.1$. After two iterations, the linear problems cannot be solved.

For our approach we start the homotopy-Newton-multigrid method with large parameters $\eta_{\text{start}} = \epsilon_{\text{start}} = 0.5$ on a coarse mesh with only 1551 elements. The algorithm is run until both homotopy parameters reach values below 0.005.

In Fig. 1 we collect the progress of the homotopy Newton method. About 3–5 Newton steps are necessary to reduce the residual ρ^n by four digits and to yield a reduction rate ρ^n/ρ^{n-1}, such that the homotopy parameters are reduced according to step 8 in the algorithm.

With a smaller value of the homotopy parameters, the convergence rate of the Newton method is reduced. Finally, we cannot satisfy the condition $\rho^n/\rho^{n-1} \leqslant \gamma_1$ at all. The Newton iteration is thus canceled by reaching the given tolerance τ. After mesh refinement the algorithm is restarted and the homotopy parameters can be further reduced. As plotted in Fig. 1, two sweeps of the algorithm are sufficient to reach $\eta = 0.005$ and $\epsilon = 0.005$.

3.2. Mesh refinement

To cope with the small structure of the singularity pattern within the solution, local mesh refinement is essential. However, combined with the homotopy method, it is difficult to generate meshes which are optimally adapted to the solution. For large values of the homotopy parameters, the shape, size and location of the singularities differ from the final state. Local mesh refinement based on these wrong (better intermediate) solutions would lead to meshes with refinements not suited to the problem. Thus, instead of using a feedback process controlled by a posteriori error estimators (See [4] for the dual weighted residual method) we control the mesh by tracking the singularity pattern.

For large values of the homotopy parameters we only use global mesh refinement. This way, we do not introduce numerical falsification of the singularity structure. Once these parameters are small enough (for

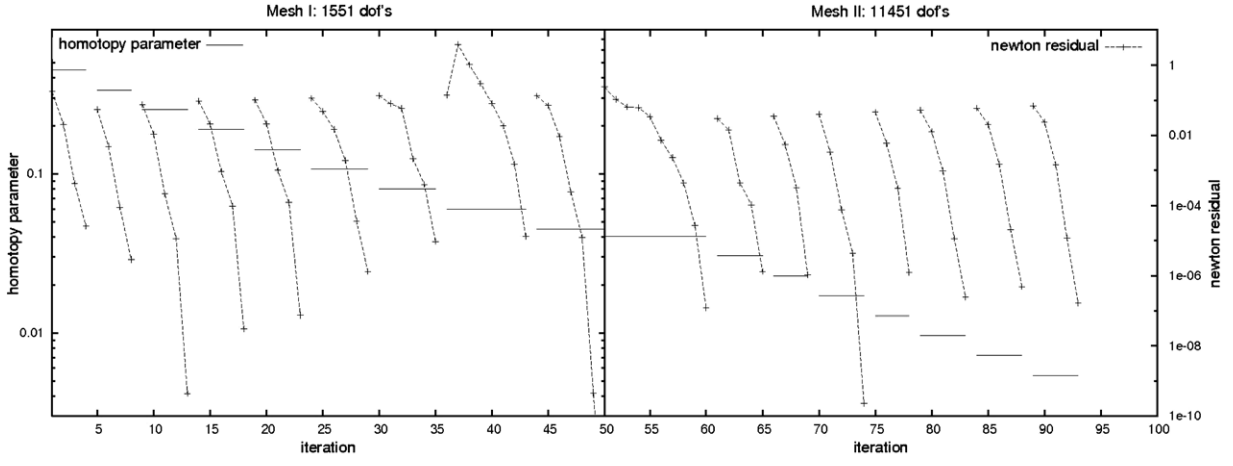

Fig. 1. Progress of the homotopy method. The horizontal solid lines indicate the value of the parameters η and ϵ, the dotted lines the residuals of the Newton iteration. The first half of the plot is done on a mesh with 1 551 degrees of freedom, the second on a mesh with 11 451 degrees of freedom.

our examples we take a limit of about 0.1 for ϵ and η) and the mesh contains at least about 10 000 elements (in 3D), we start local refinement. Here, we refine all elements, where the length of the vectors is below a certain threshold, for example 0.7. As long as the homotopy parameters are still large and diffusion is dominant, the regions of refinement are wider. For small values we get a very sharp resolution of the singularities without wasting elements.

For a final mesh control we use the dual weighted residual method (See [5]) and estimate the error according to the energy functional:

$$|E(\mathbf{u}) - E(\mathbf{u}_h)|, \quad \text{with } E(\mathbf{u}) = \int_\Omega |\nabla \times \mathbf{u}|^2 + \epsilon |\nabla \mathbf{u}|^2 + \frac{1}{4\eta}(|\mathbf{u}|^2 - 1)^2 \, \mathrm{d}\mathbf{x}.$$

With the solution $\mathbf{z} \in V_{0h}$ of the additional *dual problem* defined by

$$a'_u(\mathbf{u})(\mathbf{v}, \mathbf{z}) = E'_u(\mathbf{u})(\mathbf{v}), \quad \forall \mathbf{v} \in V_{0h}, \tag{12}$$

where $a'_u(\mathbf{u})(\mathbf{v}, \mathbf{z})$ is again the Frechet derivative (11), now with $\mathbf{z}$ and ϕ exchanged. The right hand side $E'_u(\cdot)(\cdot)$ is the derivative of the *error functional*, in our case of the energy functional:

$$E'_u(\mathbf{u})(\mathbf{v}) := \frac{\mathrm{d}}{\mathrm{d}t} E(\mathbf{u} + t\mathbf{v})\Big|_{t=0} = \int_\Omega (\nabla \times \mathbf{u}) \cdot (\nabla \times \mathbf{v}) + \epsilon \nabla \mathbf{u} : \nabla \mathbf{v} + \frac{1}{\eta}(|\mathbf{u}|^2 - 1)\mathbf{u} \cdot \mathbf{v} \, \mathrm{d}\mathbf{x}.$$

The definition of the dual problem (12) directly follows from an optimization approach for a posteriori error estimation. See [5] for details. The dual solution $\mathbf{z}$ acts as a sensitivity for the regarded error functional. In our case, $\mathbf{z}$ indicates regions of interest important for reaching a good accuracy in the energy. With the discrete solution $\mathbf{z}_h \in V_h$ of the dual problem (12) the error can be estimated as

$$E(\mathbf{u}) - E(\mathbf{u}_h) = \frac{1}{2}\{\rho(\mathbf{u}_h)(\mathbf{z} - i_h\mathbf{z}) + \rho^*(\mathbf{u}_h, \mathbf{z}_h)(\mathbf{u} - i_h\mathbf{u})\} + \mathscr{R}_h^{(3)}(e), \tag{13}$$

where ρ, ρ^* are the residual of the primal and dual problem, given by

$$\rho(\mathbf{u})(\mathbf{v}) = -a(\mathbf{u})(\mathbf{v}),$$
$$\rho^*(\mathbf{u}, \mathbf{z})(\mathbf{v}) = E'_u(\mathbf{u})(\mathbf{v}) - a'_u(\mathbf{u})(\mathbf{v}, \mathbf{z}).$$

The remainder term $\mathscr{R}_h^{(3)}$ is of third order in the error. If we approximate the interpolation errors $\mathbf{u} - i_h\mathbf{u}$ (which can be done by local recovery, see [4]), the error formula (13) can be numerically expressed and local error indicators are computable by splitting the integrals in the residuals into element-wise terms.

The solution of the discrete dual problem introduces additional numerical effort. However, the dual problem is always a linear problem and by far easier and quicker so solve than the primal one.

Considering the 3D examples presented in later sections, the savings by local mesh refinement are huge. For the configuration $p_0 = 1$ and $p_1 = 3$ (see Fig. 9) we have used 500,000 elements in 8 refinement sweeps.

To reach the same element-size with global mesh refinement, $7.8^8 \approx 100{,}000{,}000$ elements would be necessary. Here the coarse mesh contains 7 elements.

4. Simulating molecule orientations of liquid crystals

In this section we will find the equilibrium solution (or molecule orientation) of the liquid crystal model using the adaptive Newton-multigrid-homotopy finite element method discussed in the previous section. We will first consider 2D cases with Ω being a square in order to compare the results of our method with existing ones. We will then give solutions for 3D cases on various 3D domains. Our numerical experience shows that the method is very robust for this liquid crystal model.

4.1. The molecule orientation on a square slab

We consider a square domain $\Omega = (0,1) \times (0,1)$ and rotational boundary conditions $\mathbf{u} = \mathbf{g} = (\cos(p\theta), \sin(p\theta))$, where p is an integer, $\cos(\theta) = (x - 1/2)/r$, $\sin(\theta) = (y - 1/2)/r$, $r = \sqrt{(x - 1/2)^2 + (y - 1/2)^2}$

and x and y are taken on the boundary of the domain Ω. The initial values are obtained using the same formula of the boundary value function $\mathbf{g}$ except that for the initial values (x, y) is taken in the whole domain Ω.

The computational results with $\epsilon = \eta = 0.001$ are depicted in Fig. 2. In [14] the cases with $p = 1$, 2 and 3 are also calculated based on the standard gradient flow plus operator splitting. The results look similar to the results in [14], but the position of singularity is not completely the same. By calculating the energy $E(\mathbf{u}) = J_\epsilon(\mathbf{u}) + \frac{1}{4\eta}\int_\Omega (|\mathbf{u}|^2 - 1)^2$ we find that the equilibrium solution reported here has a lower energy. So the adaptive Newton-multigrid-homotopy method gives a better minimizer. Another thing we observe from our computing experience with the method is: it seems that the energy is decreasing in most cases of this Newton's iterative process for various choices of ϵ and η. To illustrate this we just record the energy sequence for $p = 2$ with $\epsilon = \eta = 0.003$ and 0.001 and $p = 3$ with $\epsilon = \eta = 0.001$ and 0.003 in Table 1. There is only one Newton step in the case of $p = 2$ with $\epsilon = \eta = 0.001$ where the energy is not decreasing. All above results suggest that our method works very well to the liquid crystal model.

4.2. Molecule orientations in typical 3D domains

We first consider a cubic domain $\Omega = [0, 1] \times [0, 1] \times [0, 1]$. In [14] a 2D solution on a square domain with the normal boundary condition was shown. The singularities took place on two diagonal lines of the square. It is expected that in a 3D cubic domain with the normal boundary condition singularities would take place on the diagonal surfaces between four diagonal lines of the cube. Fig. 3 depicts the solution and shows that the expectation is indeed correct. Note that in all 3D figures below you will see some black regions. They are the iso-surface at the arrow size = 0.2. Since near the singularity region our unit length constraint for the arrow size cannot be maintained well and the arrow size usually drops from one to something close to zero. So the iso-surface with the arrow size = 0.2 may help to characterize the singularity.

In a 2D rectangular domain with the normal boundary condition, do singularities still locate at diagonal lines of the domain? In [14] the computational results show that this is not the case. The singularity pattern

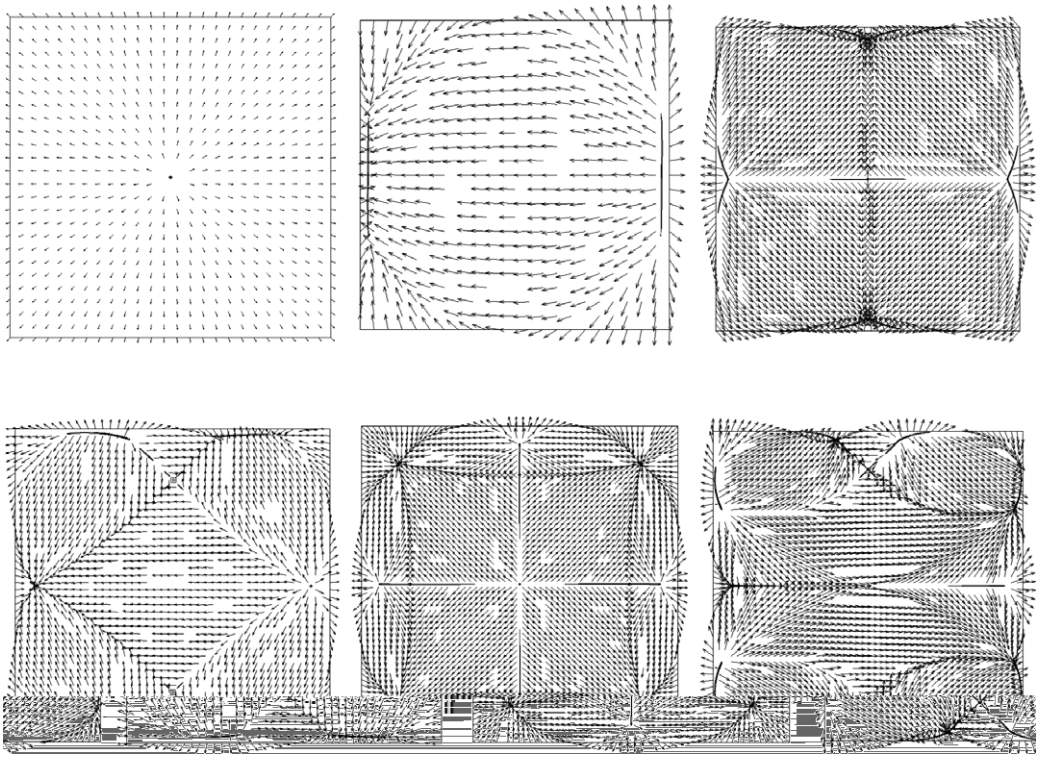

Fig. 2. Director fields on a square liquid crystal slab with $p = 1$, 2, 3, 4, 5 and 6.

Table 1
Decary of the energy throughout the Newton iteration for different boundary conditions and different values for ϵ and η

Number of Newton iterations	Energies with $p = 2$		Energies with $p = 3$	
	$\epsilon = \eta = 0.003$	$\epsilon = \eta = 0.001$	$\epsilon = \eta = 0.003$	$\epsilon = \eta = 0.001$
1	1.727736563	2.639535561	3.536462942	127.1845346
2	1.702991477	2.621166	3.367788263	27.72430021
3	1.65331395	2.571956713	3.344516427	8.93841186
4	1.648313641	2.432146793	3.335869516	5.498112348
5	1.648010467	2.386859543	3.33440511	5.148077563
6	1.648007077	2.151061622	3.333985585	4.88226389
7	1.648007076	2.038938299	3.333856107	4.657143667
8	1.648007076	1.95062986	3.333789858	4.367119492
9		1.91007785	3.333778201	4.09221224
10		1.905052784	3.333777645	3.951007037
11		1.90042532	3.333777643	3.908572077
12		1.897019366		3.906280193
13		1.891085774		3.906250584
14		2.312036616		3.906250556
15		1.825133463		3.906250556
16		1.739602113		
17		1.727318257		
18		1.726643006		
19		1.726636736		
20		1.726636735		

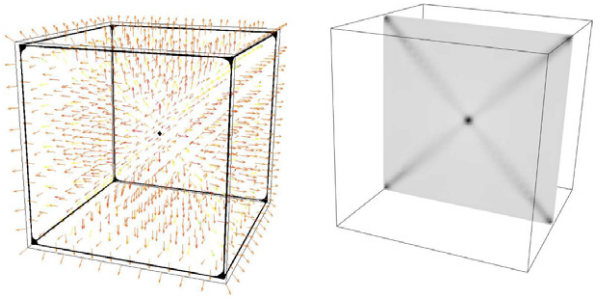

Fig. 3. Molecule orientation on a cube with the normal boundary (right: a cross-section look).

includes half diagonal lines of squares corresponding to two shorter sides plus the central line connecting them (see the left figure of Fig. 4). In a 3D parallelepiped domain $\Omega = [0, 2] \times [0, 1] \times [0, 1]$, we might expect from the 2D result that singularities are on diagonal surfaces of cubes corresponding to two smaller side surfaces of the domain plus the central surface connecting them (see the right figure of Fig. 4). For convenience of description later we will call this "expected" possible molecule orientation as a 2D-induced state. However, it seems that the 3D case may be essentially different when ϵ and η are small. The molecule orientation we obtain is not the same as the 2D-induced state.

The molecule orientation we obtain is depicted in Fig. 5. To show that our computed state is more likely to be true (i.e. having lower energy) than the 2D induced state (i.e. the right figure in Fig. 4) we can compute the energy J_ϵ as defined in (4) or J_ϵ plus the penalty term (i.e. the energy E defined before Eq. (12)) for these two different molecule orientations. Taking $\epsilon = \eta = 0.005$ we list the energies in Table 2. We see that our computed state is at a much lower energy state although it gives a quite different singularity pattern from the 2D induced one. We can actually use the 2D induced state as the initial guess of the Newton's method and observe that after ten iterations the Newton method converges to our computed state again with a lower energy. We record singularity patterns in the middle cross-sectional plane at the zeroth, first, second, and tenth iterations below in Fig. 6 to see how the singularity pattern in the middle plane is formulated.

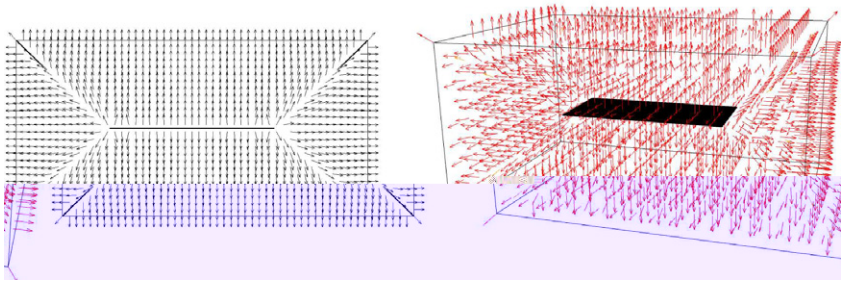

Fig. 4. The molecule orientation in a 2D rectangular with the normal boundary condition and the 2D induced molecule orientation in a 3D parallelepiped domain.

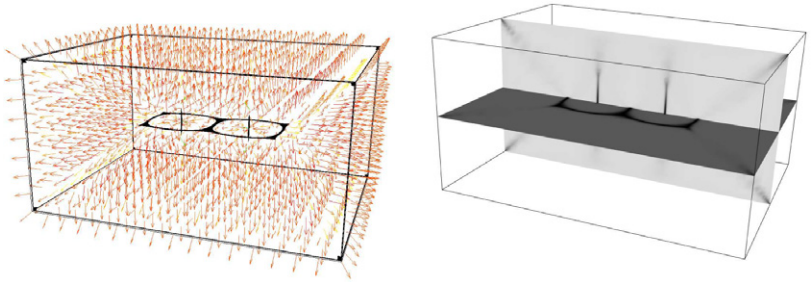

Fig. 5. The computed molecule orientation in a 3D parallelepiped domain.

Table 2
Energies for the induces initial state and for the computed state for the parallelelepiped domain using small values of η and ϵ

Molecule orientations	Energy J_ϵ	Energy E
The 2D induced state	29.951144	32.225007
The computed state	3.584933	5.653934

The elliptic or ellipsoidal domain is another interesting case. Unlike rectangular or parallelepiped domains it has a smooth boundary. For the purpose of comparison we depict the molecule orientations in an ellipse and an ellipsoid with the normal boundary condition (see Fig. 7). In [18] the asymptotic behavior of minimizers of the functional (6) is studied provided that $\nabla \times \mathbf{u} = 0$. They found that for the 2D elliptic domain the defect set (singularities) is a straight line segment ending at centers of curvature of $\partial\Omega$. In [14] this singularity line is not clearly seen perhaps because ϵ and mesh size are not small enough. With the adaptive homotopy technique developed here we are able to largely reduce ϵ and mesh size and we do observe the singularity line segment in the left figure of Fig. 7. In the ellipsoid we see such a singularity line as well. So our computational result may provide some evidence that in the limiting case a minimizer may indeed be non-rotational (i.e. $\nabla \times \mathbf{u} = 0$).

It would also be interesting to see 3D molecule orientations and their singularity patterns under 3D rotational boundary conditions $\mathbf{u} = (\sin(p_0\theta)\sin(p_1\phi), \sin(p_0\theta)\cos(p_1\phi), \cos(p_0\theta))$, where

$$\sin(\theta) = \frac{\sqrt{x^2+y^2}}{r}, \quad \cos(\theta) = \frac{z}{r}, \quad r = \sqrt{x^2+y^2+z^2},$$
$$\sin(\phi) = \frac{x}{\sqrt{x^2+y^2}}, \quad \cos(\phi) = \frac{y}{\sqrt{x^2+y^2}},$$

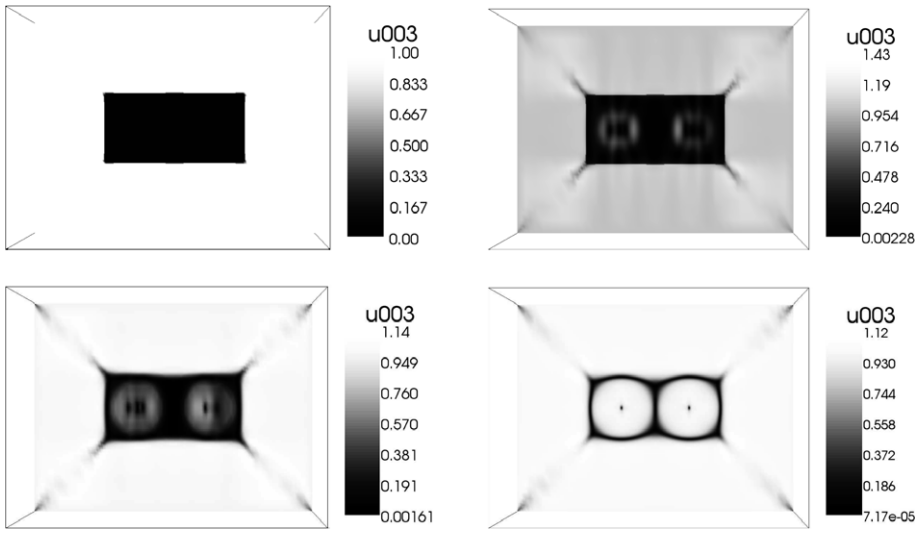

Fig. 6. Formation of the singularity pattern in the middle plane starting from the 2D induced state.

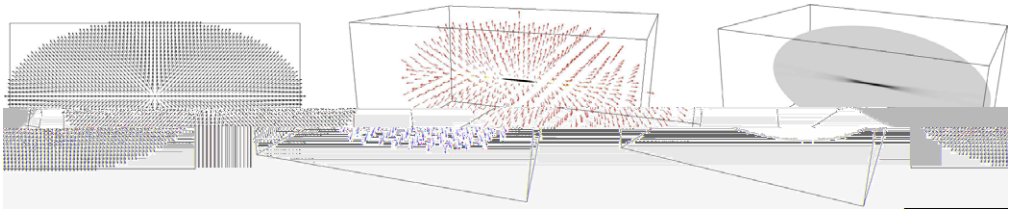

Fig. 7. Molecule orientations in an ellipse and an ellipsoid (including a cross-section look of the ellipsoidal case at the right) with the normal boundary condition.

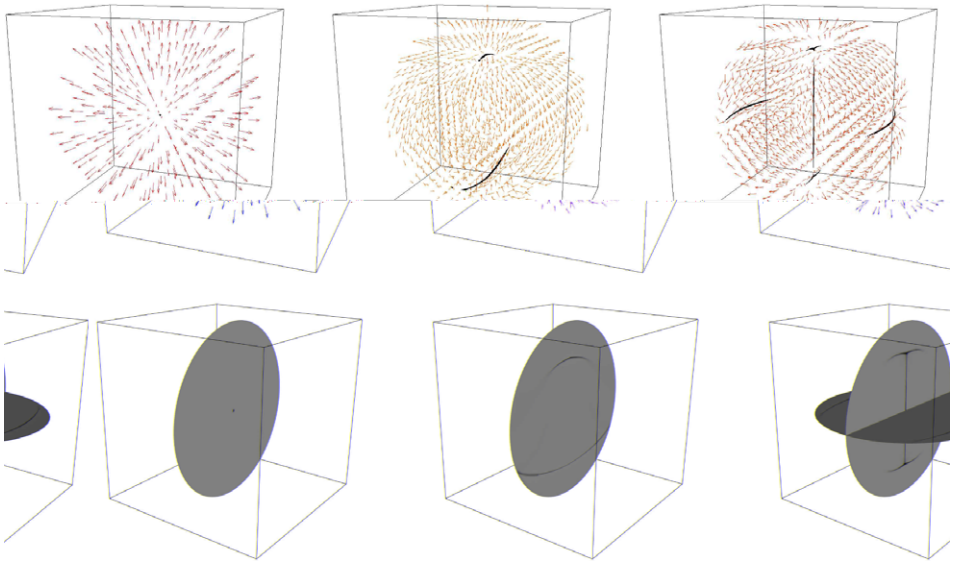

Fig. 8. Molecule orientations on a spherical liquid crystal domain with $p_0 = 1$, 2 and 3 and $p_1 = 1$ (bottom: a cross-section look of the singularity pattern).

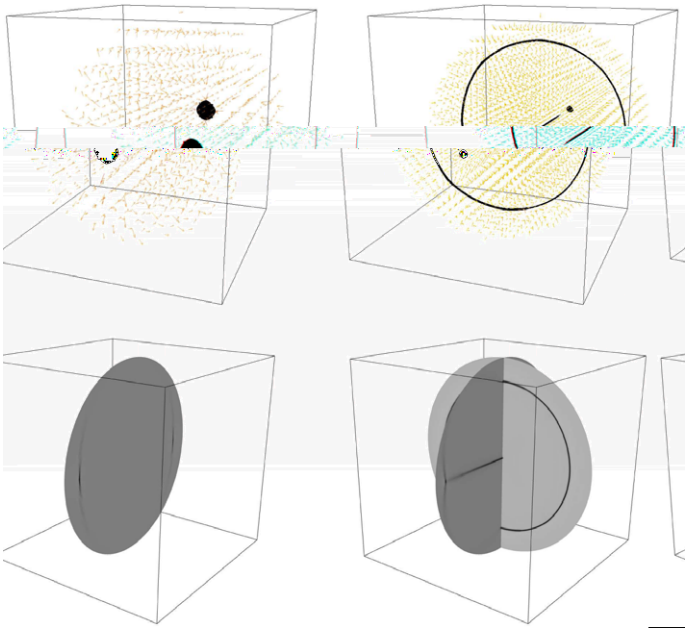

Fig. 9. Molecule orientations on a spherical liquid crystal domain with $p_0 = 1$ and $p_1 = 2$ and 3 (bottom: a cross-section look of the singularity pattern).

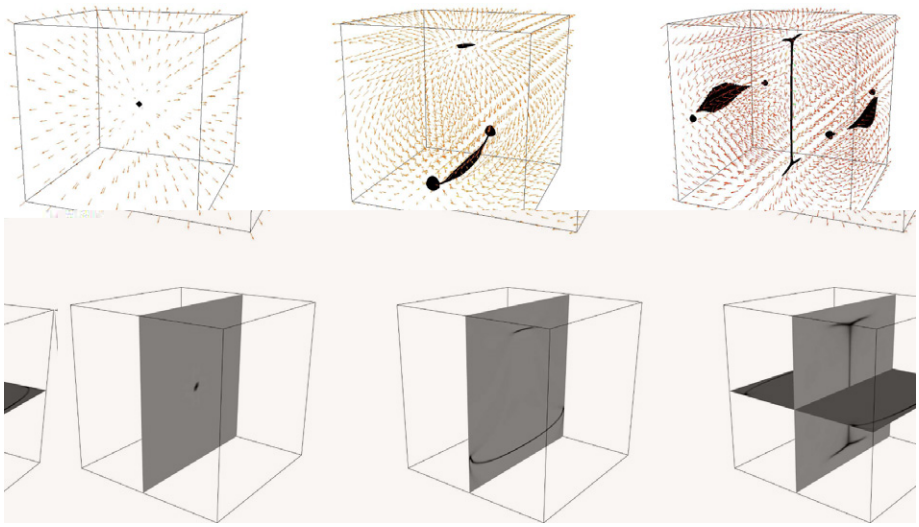

Fig. 10. Molecule orientations on a cubic liquid crystal domain with $p_0 = 2$ and 3 and $p_1 = 1$ (bottom: a cross-section look of the singularity pattern).

p_0 and p_1 are integers and (x, y, z) taken values on the boundary. The initial values are obtained by using the same formula of the boundary condition but (x, y, z) being taken values inside of the domain. We compute the solution in both spherical (smooth) (see Figs. 8 and 9) and parallelepiped (non-smooth) (see Figs. 10 and 11) domains. We shall use approximately 500,000 finite elements and take ϵ and η as small as 0.005 in all the 3D computation. The singularity patterns for 3D liquid crystals may be quite different from 2D ones.

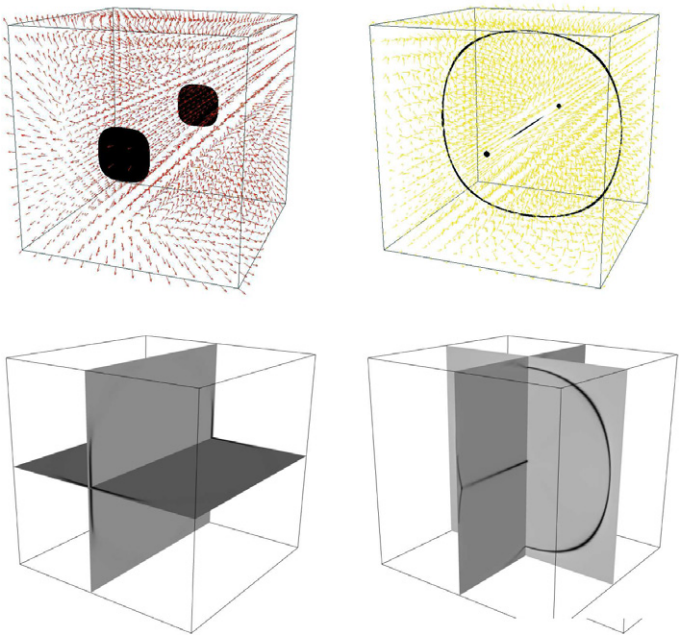

Fig. 11. Director fields on a cubic liquid crystal domain with $p_0 = 1$ and $p_1 = 2$ and 3 (bottom: a cross-section look of the singularity pattern).

Acknowledgement

The work of Lin is partially supported by NUS Academic Research Grant no. R-146-000-053-112.

References

[1] F. Alouges, A new algorithm for computing liquid crystal stable configurations: The harmonic mapping case, SIAM J. Numer. Anal. 34 (1997) 1708–1726.
[2] P. Aviles, Y. Giga, A mathematical problem related to the physical theory of liquid crystal configurations, Proc. Centre Math. Anal. Austral. Nat. Univ. 12 (1987) 1–16.
[3] P. Aviles, Y. Giga, On lower semicontinuity of a defect energy obtained by a singular limit of the Ginzburg–Landau type energy for gradient field, Proc. Roy. Soc. Edinburgh Sect. A 129 (1999) 1–17.
[4] R. Becker, R. Rannacher, A feed-back approach to error control in finite element methods: basic analysis and examples, East-West J. Numer. Math. 4 (1996) 237–264.
[5] R. Becker, R. Rannacher, An optimal control approach to a posteriori error estimation in finite element methods, in: A. Iserles (Ed.), Acta Numerica 2000, Cambridge University Press, 2001, pp. 1–102.
[6] M. Braack, T. Richter, Solutions of 3D Navier–Stokes benchmark problems with adaptive finite elements, Comput. Fluids 35 (2006) 372–392.
[7] R. Becker, M. Braack, T. Richter, B. Vexler, Gascoigne – Adaptive Finite Element Toolkit, University of Heidelberg. <http://www.gascoigne.de>.
[8] Robert Cohen, San-Yih Lin, Mitchell Luskin, Relaxation and gradient methods for molecular orientation in liquid crystals, Comput. Phys. Comm. 53 (1989) 455–465.
[9] R. Cohen, R. Hardt, D. Kinderlehrer, S.-Y. Lin, M. Luskin, in: J.L. Ericksen, D. Kinderlehrer (Eds.), Theory and Applications of Liquid Crystals, IMA Volumes in Mathematics and its Applications, vol. 5, Springer-Verlag, Berlin, 1987.
[10] P.G. de Gennes, An analogy between superconductors and smectics A, Solid State Commun. 10 (1972) 753–756.
[11] P.G. de Gennes, J. Prost, The Physics of Liquid Crystals, second ed., Oxford Science Publications, Oxford, 1993.
[12] Q. Du, B.Y. Guo, J. Shen, Fourier spectral approximation to a dissipative system modeling the flow of liquid crystals, SIAM J Numer. Anal. 39 (3) (2002) 735–762.
[13] F.C. Frank, On the theory of liquid crystals, Discuss. Faraday Soc. 25 (1958) 19–28.
[14] R. Glowinski, P. Lin, X.B. Pan, An operator-splitting method for a liquid crystal model, Comput. Phys. Comm. 152 (2003) 242–252.
[15] R. Glowinski, P. Le Tallec, Augmented Lagrangian and Operator-Splitting Methods in Nonlinear Mechanics, SIAM, 1989.

[16] R. Hardt, D. Kinderlehrer, Mathematical questions of liquid crystal theory, in: J.L. Ericksen, D. Kinderlehrer (Eds.), Theory and Applications of Liquid Crystals, IMA Volumes in Mathematics and its Applications, vol. 5, Springer-Verlag, 1987, pp. 151–184.
[17] R. Hardt, D. Kinderlehrer, F.H. Lin, Existence and partial regularity of static liquid crystal configurations, Comm. Math. Phys. 105 (1986) 547–570.
[18] W. Jin, R.V. Kohn, Singular perturbation and the energy of folds, J. Nonlinear Sci. 10 (2000) 355–390.
[19] F.H. Lin, Nonlinear theory of defects in nematic liquid crystals, phase transitions and flow phenomena, Comm. Pure Appl. Math. 42 (1989) 789–814.
[20] P. Lin, C. Liu, Simulation of singularity dynamics in liquid crystal flows: a C^0 finite element approach, J. Comp. Phys. 215 (1) (2006) 348–362.
[21] C. Liu, Noel J. Walkington, Approximation of liquid crystal flows, SIAM J Numer. Anal. 37 (2000) 725–741.
[22] X.B. Pan, Y. Qi, Asymptotics of minimizers of variational problems involving curl functional, J. Math. Phys. 41 (2000) 5033–5063.